RESEARCH

Multilevel resistive switching memory based on a $CH_3NH_3PbI_{3-x}Cl_x$ film with potassium chloride additives

Fengzhen Lv*, Kang Ling†, Tingting Zhong, Fuchi Liu*, Xiaoguang Liang, Changming Zhu, Jun Liu and Wenjie Kong

*Correspondence:
lvfzh17@mailbox.gxnu.edu.cn,
liufuchi@gxnu.edu.cn
College of Physics and Technology, Guangxi Normal University, Yucai Road, Guilin, China
†Equal contributor

Abstract

High-quality $CH_3NH_3PbI_{3-x}Cl_x$ (MAPIC) films were prepared using potassium chloride (KCl) as an additive on indium tin oxide(ITO)-coated glass substrates using a simple one-step and low-temperature solution reaction. The Au/KCl-MAPIC/ITO/Glass devices exhibited obvious multilevel resistive switching behavior, moderate endurance, and good retention performance. Electrical conduction analysis indicated that the resistive switching behavior of the KCl-doped MAPIC films was primarily attributed to the trap-controlled space-charge-limited current conduction that was caused by the iodine vacancies in the films. Moreover, the modulations of the barrier in the Au/KCl-MAPIC interface under bias voltages were thought to be responsible for the resistive switching in the carrier injection trapping/detrapping process.

Keywords: Tri-state resistive switching behavior; KCl-doped MAPIC films; iodine vacancies; trap-controlled SCLC conduction mechanism

Introduction

As a result of the rapid development of the information storage industry, modern memory technologies have attracted wide attention. Among various types of memories, resistive switching random access memory (ReRAM) is considered one of the most competitive next-generation non-volatile data storage devices owing to its simple architecture, fast programming speed, high density, and good stability [1, 2]. In order to enhance the storage density, recently, multilevel memory with the unique ability to store more than 2-bits in a single cell, which is required in ReRAM, has been developed [3, 4]. The ability of multilevel storage has been reported for various inorganic materials [5, 6, 7, 8]. Although they possess excellent memory performance, the complex fabrication process and rigidity hinder their development for ReRAM. Most recently, organic-inorganic hybrid materials have attracted a great deal of attention due to their high flexibility, tunable band gaps, and large absorption coefficients [9, 10]. Among hybrid materials, organometal halide perovskites (OHPs), which owns well-optimized film morphology and extremely long carrier diffusion lengths, have attracted the most attention for use as flexible and versatile ReRAM [11, 12, 13, 14, 15]. However, resistive switching devices based on OHPs suffer from poor endurance and retention performance. In the most recent studies, potassium halides have been proposed as an additive to reduce the grain boundaries, compensate for defects in OHPs, and provide improved optoelectronic

properties [16, 17, 18]. Nevertheless, the resistive switching behavior in potassium halide-doped OHPs has not been extensively reported.

In this study, we prepared $CH_3NH_3PbI_{3-x}Cl_x$(MAPIC) films with potassium chloride (KCl) additive on indium tin oxide (ITO)-coated glass substrates using a one-step low-temperature solution treatment. We evaluate the non-volatile resistive switching effect in the Au/KCl-MAPIC/ITO/Glass memory device. Distinct multilevel resistive switching behavior is achieved by the Au/KCl-MAPIC/ITO/Glass device at different set voltages (V_{SET}). The electrical conductive behavior is primarily attributed to the trap-controlled space-charge-limited current (SCLC) conduction mechanism based on the variation of iodine vacancies ($V_I^{\cdot}$) in the films. Moreover, the modulations of the barrier at the Au/KCl-MAPIC interface under bias voltages are thought to be responsible for the resistive switching behavior.

Experiment

Prior to growing the samples, the ITO/Glass substrates (10 mm×10 mm, Luoyang Guluo Glass Co., Ltd.) were cleaned sequentially in acetone, isopropyl alcohol, deionized water and were dried under a nitrogen gas flow. The perovskite precursor solution was prepared by combining lead iodide (PbI_2, 98%, 370 mg), methylammonium iodide (MAI, 99.5%, 130 mg), and methylammonium chloride ((MACl, 98%, 20mg) with anhydrous N,N-dimethylformamide (DMF, >99.5%, 1 mL). Subsequently, KCl (>99.5%, 7 mg) was added to the mixed solution. The yellowish precursor solution (0.8 M) was stirred more than 6 h in an argon-filled glove box. Then, the precursor solution was spin-coated on ITO/Glass substrates at 3000 rpm for 30 s, as shown in Fig. 1(a). After 6 s of spin coating, anhydrous chlorobenzene (100 μL) was dropped rapidly onto the surface of the intermediate phase film. The film immediately changed from pale yellow to nut-brown [Fig. 1(b) and 1(c)]. Finally, the sample was heated on a hot plate at 100 °C for 10 min, as shown in Fig. 1(d).

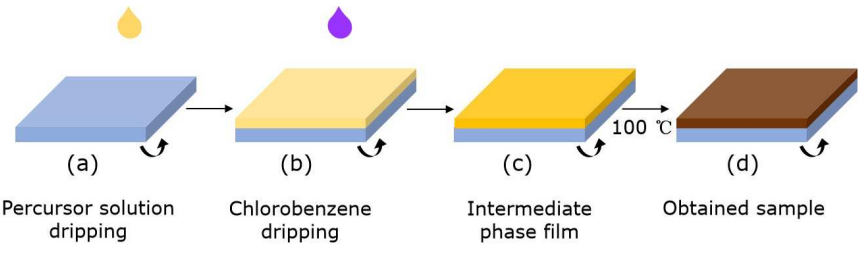

Figure 1 Solvent engineering procedure for preparing the KCl-doped MAPIC film on the ITO-coated glass substrate.

Characterization

The phase structure of the MAPIC films was investigated by X-ray diffractometry (XRD; MiniFlex600, Rigaku, JPN). The chemical element analysis of the films was performed using X-ray photoelectron spectroscopy/ultraviolet photoelectron spectroscopy (XPS/UPS; ESCALAB250Xi, Thermo Fisher Scientific, USA) using Al Kα radiation and a He I source with 21.22 eV. The morphology of the MAPIC

films was assessed with scanning electron microscopy (SEM; FEI Quanta 200). The current-voltage (*I-V*) characteristics of the KCl-MAPIC films were examined using a Keithley 2400 SourceMeter.

Results and discussion

Figure 2(a) shows the crystallization of the KCl-doped MAPIC films. The sharp peaks indexed as (110), (220), and (330) indicate the typical tetragonal phase with high crystallinity in the film [11, 19]. Figure 2(b) displays the XPS wide spectrum of the perovskite film. C, Pb, I, N, and K are present in the films. However, the full spectrum scan shows negligible amounts of Cl. This finding is consistent with the results of previous reports, which demonstrated that Cl was present in the intermediate phase of the MAPIC film but easily escaped during the annealing process; therefore, the presence of Cl is rare in the final product [19, 20]. Figure 2(c) presents the top-view SEM image of the KCl-MAPIC film. It is found that the perovskite film exhibits high coverage and is dense. The layer with a dense thickness of ∼200 nm is clearly visible in Fig. 2(d).

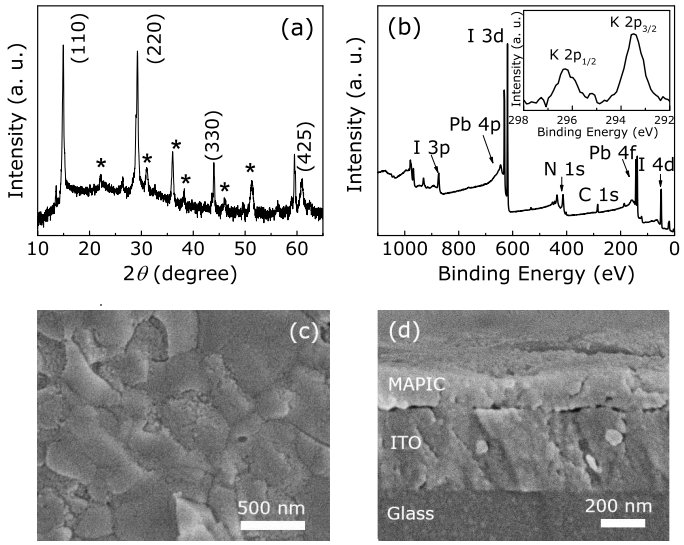

Figure 2 (a) Symmetric XRD longitudinal ω-2θ scans of the as-grown KCl-doped MAPIC films on the ITO-coated glass substrate. $\star$ represents peaks of the ITO/Glass substrate. (b) XPS spectrum of the pervoskite films. The inset displays the core-level XPS spectrum of K. (c) The top-view SEM image of films. (d) The cross-sectional SEM image taken in an arbitrary portion of the sample.

Figure 3 depicts the semi-logarithmic plots of the *I-V* curve of the Au/KCl-MAPIC/ITO/Glass devices under positive and negative voltage sweeps. A schematic of the device used for the measurements is shown in the inset of Fig. 3. Au electrodes with diameters of 300 μm were deposited by magnetron sputtering on the surface of the KCl-doped MAPIC film using a shadow mask. Initially, the device is in a high-resistance state (HRS, i.e., the OFF state) and then the current increases gradually as the positive voltage increases. Subsequently, the memory device transitions from the HRS to different low-resistance states (LRSs, i.e., the ON states) under the two V_{SETs} of 0.8 V and 1 V. The *I-V* characteristics indicate that the Au/KCl-MAPIC/ITO/Glass device has the multilevel storage potential.

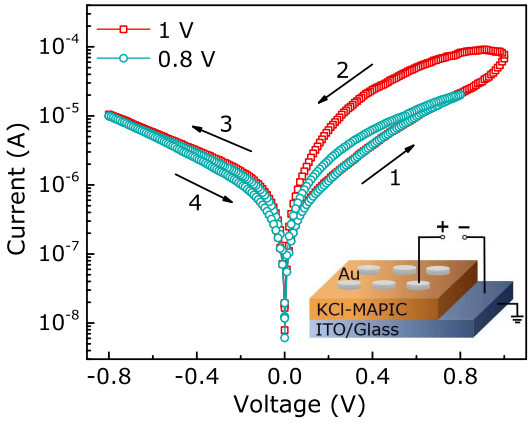

Figure 3 The I-V characteristic of Au/KCl-MAPIC/ITO/Glass devices under the sweeping voltage of 0 V→0.8 V/1 V→-0.8 V→0 V. The numbers and arrows represent the voltage sweeping sequences and directions, respectively. The inset exhibits the schematic device structure for the measurement.

The retention and endurance properties of the Au/KCl-MAPIC/ITO/Glass cells were characterized to test their potential use in a memory device and determine the multilevel-storage stability and reliability of the device. As shown in Fig. 4(a), electric pulses of V_{SETs} and reset voltage (V_{RESET}) were alternately applied to the device (pulse width=0.4 s). The different resistances can be maintained for up to 140 cycles under different V_{SETs} of 0.8 V and 1 V. The HRS at a reading voltage (V_{r}) of 0.22 V is defined as the "OFF state". The two different low resistance states (LRSs) are defined as levels 1 and 2. When the V_{r} is consistently applied, the resistances of each state are stable for over 1000 s as shown in Fig. 4(b). Therefore, the potential of the multilevel memory has been demonstrated in the Au/KCl-MAPIC/ITO device.

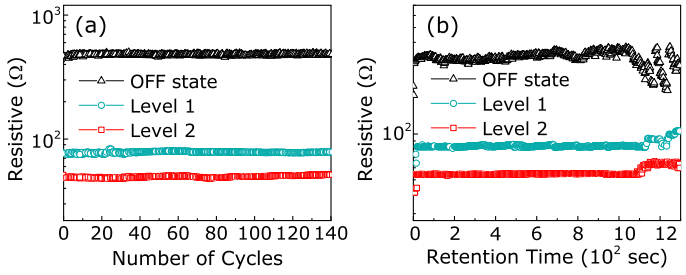

Figure 4 (a) Pulse cycles up to 140 times and (b) time up to about 1200 s for HRS and LRS measurements in the Au/KCl-MAPIC/ITO/Glass device at room temperature.

A deep understanding of the switching mechanisms is indispensable for improving future applications of KCl-doped MAPIC films for ReRAM. The resistive switching behavior has been explained by various conduction mechanisms such as the Schottky emission, conductive filaments, hopping conduction, and SCLC. These mechanisms can be distinguished by creating an isothermal logarithmic plot of the *I-V* correlation [14, 15, 21, 22]. We plotted the *I-V* curves in a double-log scale as shown in Fig. 5. In the initial positive bias region from 0 to 0.2 V, the *I-V* relationship has a

slope of ∼1.01, demonstrating that the *I*-*V* characteristics follow Ohm's law. As the positive bias increases (0.2 V∼0.6 V), the *I*-*V* relationship is $I \propto V^2$, which is the well-known SCLC controlled by single shallow traps. When the forward bias reaches the trap-filled limit voltage (V_{TFL}), the current increases sharply and the slope is ∼8.20, and the *I*-*V* relationship obeys the exponential distributed trap-controlled SCL conduction. When the bias reaches V_{SET}, the resistance changes into the LRS. Even though the positive bias decreases, the resistance still maintains the LRS. As illustrated in Fig. 5(b), when the bias sweeps reversely, the Au/KCl-MAPIC/ITO device remains in the LRS, whereas the negative bias crosses V_{RESET} and reaches V^*_{TFL}; the current decreases as the voltage decreases and the relationship of *I*-*V* recovers $I \propto V^2$.

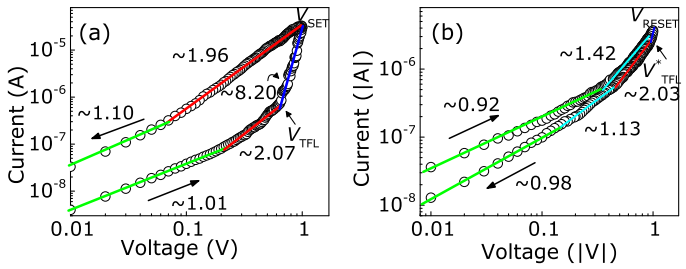

Figure 5 The fitted lines of the double logarithmic I-V plots for the (a) OFF state and (b) ON state. The arrows indicate the sweeping direction.

It is well known that many types of defects exist in OHPs, such as vacancies (V'_{Pb}, V'_{MA}, $V_I^{\cdot}$) and interstitials (Pb_i, MA_i, I_i) [23, 24]. Thereinto, halide vacancies are readily formed in the organic-halide hybrid perovskite films during the solution-based film-deposition process [25]. $V_I^{\cdot}$ can migrate at the lowest activation energy of ∼0.58 eV [26]. Thus, $V_I^{\cdot}$ is assumed to be a major factor in the resistive switching mechanism [27]. We obtained XPS measurements to verify this hypothesis and analyze the condition of the perovskite layer. Figure 6 illustrates the core-level XPS spectra of I and Pb. As illustrated in Fig. 6(a), the binding energy of the I $3d_{3/2}$ and I $3d_{5/2}$ peaks are 631.90 eV and 620.45 eV, respectively. The peak positions shift slightly to higher binding energy, which indicates the generation of $V_I^{\cdot}$ by heat-driven deiodination [28, 29]. The XPS result in Fig. 6(b) shows the core level Pb $4f$ spectrum. Two main peaks of Pb $4f_{5/2}$ and Pb $4f_{7/2}$ are observed at 143.18 eV and 138.21 eV, respectively; this finding is consistent with previous reports [30, 31]. It is noteworthy that additional small peaks with lower binding energies (141.41 eV and 136.60 eV) with the signature of Pb^0 were detected by XPS [31]. These results indicate that $V_I^{\cdot}$ exists in the KCl-doped MAPIC layer.

As shown in Fig. 7(a), in the low positive bias region (0< V <0.2 V), the injected carrier concentration is lower than the concentration of the thermally generated free carriers in the KCl-MAPIC layer; the Au/KCl-MAPIC/ITO device is in the HRS, and the *I*-*V* relationship follows Ohm's law:

$$j = qn\mu\frac{V}{d} \tag{1}$$

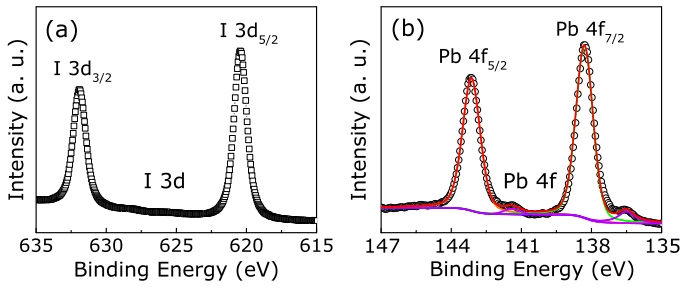

Figure 6 XPS spectra of the KCl-doped MAPIC films, (a) I 3d and (b) Pb 4f photoemission spectra with peak fitting.

where j is the transport current density, q is the electric charge, n is the density of the free electrons in thermal equilibrium, μ is the carrier mobility, V is the applied voltage and d is the film thickness. As the forward voltage increases (0.2 V$< V < V_{\mathrm{TFL}}$), the electrons injected from the bottom electrode are trapped by $\mathrm{V_I^{\cdot}}$ [Fig. 7(b)]. In this process, the *I*-*V* relationship corresponds to the following functional form:

$$j = \frac{9}{8}\theta\varepsilon_0\varepsilon_r\mu\frac{V^2}{d^3} \tag{2}$$

where θ is the fraction of free carriers, ε_0 is the permittivity of the free space, and ε_r is the dielectric constant of the insulator. This conduction behavior shows that the SCL conduction is controlled by a single shallow trap that is close enough to the the conduction band. As the positive bias increases further, the voltage reaches V_{TFL}, the electrons trapped are activated and emitted into the top Au electrode. And then, additional injected electrons fill the empty trap immediately. In this process, the traps are filled up, and the film remains in the trap-filled state. Subsequently, the current behavior should directly switch to the trap-free SCL conduction; the current increases exponentially with the voltage. The aforementioned process is known as the trapping process. When the positive bias reaches V_{SET}, the Au/KCl-MAPIC/ITO cell finally reaches the LRS [Fig. 7(c)]. The charge traps are filled over time, and the electrons can then hop from trap-to-trap. As the positive voltage decreases, the injected electrons cannot fill the trap but $\mathrm{V_I^{\cdot}}$ maintains a filled-state; the electron concentration is high, and the device remains in the LRS. As exhibited in Fig. 7(d), when the bias sweeps reversely, the trapped electrons cannot be released from the $\mathrm{V_I^{\cdot}}$ immediately; the carrier concentration remains at a high level, and the device remains in the LRS. As the negative voltage reaches and crosses V_{RESET}, the trapped electrons are drawn out from the traps [Fig. 7(e)]. When the reverse bias decreases to V^*_{TFL}, the current behavior changes from the trap-filled SCL conduction to the SCL conduction controlled by a single shallow trap. As the negative voltage further decreases, the electrons cannot fill the trap; therefore, the film returns to the unoccupied trap state [Fig. 7(f)]. When the injected electron concentration is smaller than the equilibrium concentration, the device returns to the HRS.

Furthermore, according to reports on the transition process of the current under a bias sweep, we surmise that the bias-induced modification of the barrier height

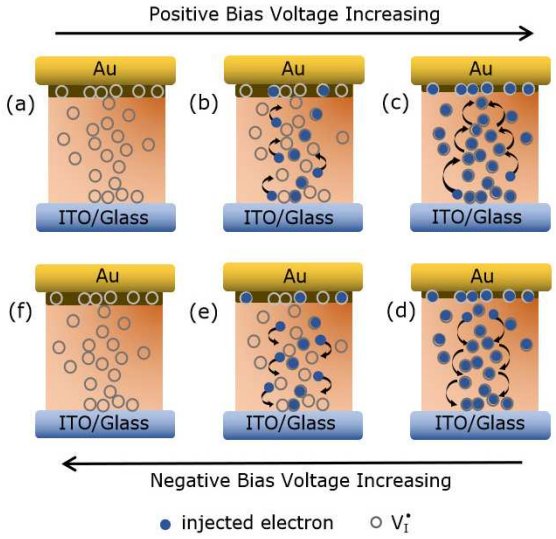

Figure 7 SThe schematic diagram of the proposed model for the resistive switching in the Au/KCl-MAPIC/ITO/Glass cell.

and/or width in the Au/KCl-MAPIC/ITO sandwiches also contributed to the resistive switching [19, 32, 33]. UPS was conducted to confirm the conjecture and examine the contact types of the electrodes/perovskite layer. Figure 8(a) and 8(b) show the cut-off regions of the KCl-MAPIC film and ITO-coated glass, respectively. The work functions of the film and substrate are calculated as 4.42 eV and 4.50 eV, respectively. These values are similar to results obtained in previous reports [19, 33, 34]. Thus, we confirm that a contact between KCl-MAPIC layer and ITO-coated glass is Ohmic due to their similar work functions. However, it is well known that the work function of Au is about 5.0 eV [19, 32]. This value is larger than that of the KCl-MAPIC film. Therefore, a barrier forms at Au/KCl-MAPIC interface. As shown in Fig. 7(b), electrons start to drift towards the Au electrode and be trapped by the $V_I^{\bullet}$ in the depletion layer near the Au/KCl-MAPIC interface under a positive voltage. When the forward voltage reaches V_{SET}, the holes are full-filled, lead to the Schottky-like barrier height and/or width lowing, and the depletion layer thickness is reduced [Fig. 7(c)]. The contact between perovskite and Au electrode becomes a quasi-ohmic contact, the device switches from the HRS to the LRS. As shown in Fig. 7(d)-(f), when the bias sweeps in reverse direction and increases to V_{RESET}, the trapped electrons are pulled out from hole traps and the barrier height recovers to the original state; an internal electric field is induced between the depletion layer and the barrier because the electrons injected from the Au electrode are obstructed by the barrier at the Au/KCl-MAPIC interface. Thus, the carrier concentration decreases in the KCl-MAPIC film and resets the resistance from the LRS to the HRS.

Conclusions

High-quality KCl-doped MAPIC films were prepared using a low-temperature one-step reaction. The Au/KCl-MAPIC/ITO/Glass device exhibited a tri-state resistive switching behavior under modulated V_{SET} at room temperature. No apparent

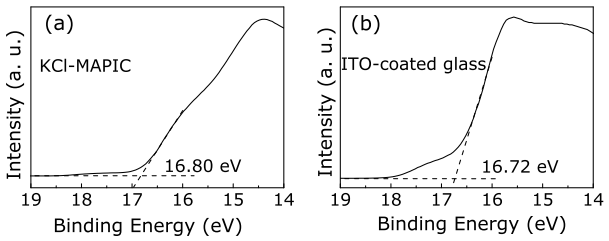

Figure 8 Cut-off regions of (a) the KCl-MAPIC film and (b) the ITO-coated glass.

degradation was observed in the HRS and LRS in this device after 1000 s and different voltage cycles, demonstrating that the Au/KCl-MAPIC/ITO/Glass cell has the potential for multilevel storage in ReRAM. The current conduction analysis revealed that the trap-controlled SCLC conduction mechanism contributed to the resistive switching in the Au/KCl-MAPIC/ITO/Glass devices. Furthermore, the modulation of the Au/KCl-MAPIC barrier under the applied bias was also responsible for the resistive state switching in the carrier injection-trapping/detrapping process.

Competing interests

The authors declare that they have no conflict of interest.

Author's contributions

Fengzhen Lv provided the conceptualization, guided the experiments, conducted the data analysis, and prepared the original draft. Kang Ling conducted the experimental process and participated the data discussion. Tingting Zhong participated in the experimental process. Fuchi Liu, Xiaoguang Liang, Changming Zhu, Jun Liu and Wenjie Kong provided guidance for the experiments and participated in the revision of the manuscript. All authors read and approved the final manuscript.

Acknowledgements

This work was financially supported by the National Natural Science Foundation of China (No.11664003), Natural Science Foundation of Guangxi Province (No. 2018GXNSFAA294021, 2018GXNSFBA281073, 2018GXNSFBA138007) and the Scientific Research and Technology Development Program of Guilin (No.2016012002).

References

1. Waser, R., Aono, M.: Nanoionics-based resistive switching memories. Nat Mater **6**, 833–843 (2007)
2. Waser, R., Dittman, R., Staikov, G., Szot, K.: Redox-based resistive switching memories–nanoionic mechanisms, prospects, and challenges. Adv Mater **21**, 2632–2663 (2009)
3. Rozenberg, M.J., Inoue, I.H., Sánchez, M.J.: Nonvolatile memory with multilevel switching: a basic model. Phys Rev Lett **92**, 1–4 (2004)
4. Wang, H., Meng, F.B., Cai, Y.R., Zheng, L.Y., Li, Y.G., Liu, Y.J., Jiang, Y.Y., Wang, X.T., Chen, X.D.: Sericin for resistance switching device with multilevel nonvolatile memory. Adv Mater **25**, 5498–5503 (2013)
5. Bae, Y.C., Lee, A.R., Lee, J.B., Koo, J.H., Kwon, K.C., Park, J.G., Im, H.S., Hong, J.P.: Oxygen ion drift-induced complementary resistive switching in homo $TiO_x/TiO_y/TiO_x$ and hetero $TiO_x/TiON/TiO_x$ triple multilayer frameworks. Adv Funct Mater **22**, 709–716 (2012)
6. Gao, C.X., Lv, F.Z., Zhang, P., Zhang, C., Zhang, S.M., Dong, C.H., Gou, Y.C., Jiang, C.J., Xue, D.S.: Tri-state bipolar resistive switching behavior in a hydrothermally prepared epitaxial $BiFeO_3$ film. J Alloy Compd. **649**, 694–698 (2015)
7. Zhou, W.P., Xiong, Y.Q., Zhang, Z.M., Wang, D.H., Tan, W.S., Cao, Q.Q., Qian, Z.H., Du, Y.W.: Multilevel resistance switching memory in $La_{2/3}Ba_{1/3}MnO_3$/0.7Pb($Mg_{1/3}Nb_{2/3}$)O_3-0.3$PbTiO_3$(011) heterostructure by combined straintronics-pintronics. ACS Appl Mater Interfaces **8**, 5424–5431 (2016)
8. Lv, F.Z., Ling, K., Wang, W.F., Chen, P., Liu, F.C., Kong, W.J., Zhu, C.M., Liu, J., Long, L.Z.: Multilevel resistance switching behavior in $PbTiO_3$/Nb:$SrTiO_3$(100) heterostructure films grown by hydrothermal epitaxy. J Alloy Compound **778**, 768–773 (2019)
9. Hwang, S.K., Lee, J.M., Kim, S.J., Park, J.S., Park, H., Ahn, C.W., Lee, K.J., Lee, T., Kim, S.O.: Flexible multilevel resistive memory with controlled charge trap B- and N-doped carbon nanotubes. Nano Lett **12**, 2217–2221 (2012)
10. Wang, H., Du, Y.M., Li, Y.T., Zhu, B., Leow, W.R., Li, Y.G., Pan, J.S., Wu, T., Chen, X.D.: Configurable resistive switching between memory and threshold characteristics for protein-based devices. Adv Funct Mater **25**, 3825–3831 (2015)

11. Yoo, E.J., Lyu, M.Q., Yun, J.-H., Kang, C.J., Choi, Y.J., Wang, L.Z.: Resistive switching behavior in organic–inorganic hybrid $CH_3NH_3PbI_{3-x}Cl_x$ perovskite for resistive random access memory devices. Adv Mater **27**, 6170–6175 (2015)
12. Lv, F.Z., Gao, C.X., Zhou, P. H -A andZhang, Mi, K., Liu, X.X.: Nonvolatile bipolar resistive switching behavior in the perovskite-like $(CH_3NH)_3FeCl_4$. ACS Appl Mater Interfaces **8**, 18985–18990 (2016)
13. Hwang, B., Lee, J.S.: Lead-free, air-stable hybrid organic–inorganic perovskite resistive switching memory with ultrafast switching and multilevel data storage. Nanoscale **10**, 8578–8584 (2018)
14. Shan, Y.Y., Lyu, Z.S., Guan, X.W., Younis, A., Yuan, G.L., Wang, J.L., Li, S., Wu, T.: Solution-processed resistive switching memories based on hybrid organic-inorganic materials and composites. Phys Chem Chem Phys **20**, 23837–23846 (2018)
15. Zhao, X.N., Xu, H.Y., Wang, Z.Q., Lin, Y., Liu, Y.C.: Memristors with organic-inorganic halide perovskites. Info Mat **1**, 183–210 (2019)
16. Zhao, W.G., Yao, Z., Yu, F.Y., Yang, D., Liu, S.Z.: Alkali metal doping for improved $CH_3NH_3PbI_3$ perovskite solar cells. Adv Sci **5**, 1–7 (2018)
17. Jalebi, M.A., Garmaroudi, Z.A., Cacovich, S., Stavrakas, C., Philippe, B., Richter, J.M., Alsari, M., Booker, E.P., Hutter, E.M., Pearson, A.J., Lilliu, S., Savenije, T.J., Rensmo, H., Divitini, G., Ducati, C., Friend, R.H., Stranks, S.D.: Maximizing and stabilizing luminescence from halide perovskites with potassium passivation. Nature **555**, 497–501 (2018)
18. Shih, C.F., Wu, H.T., Tsai, W.L., Leu, C.C.: Improvement of resistive memory properties of poly(3,4-ethylenedioxythiophene):poly(styrenesulfonate)/$CH_3NH_3PbI_3$ based device by potassium iodide additives. J Alloy Compound **783**, 478–485 (2019)
19. Zhou, F.C., Liu, Y.H., Shen, X.P., Wang, M.Y., Yuan, F., Chai, Y.: Low-voltage, optoelectronic "$CH_3NH_3PbI_{3-x}Cl_x$" memory with integrated sensing and logic operations. Adv Funct Mater **1800080**, 1–8 (2018)
20. Yu, H., Wang, F., Xie, F.Y., Li, W.W., Chen, J., Zhao, N.: The Role of Chlorine in the Formation Process of "$CH_3NH_3PbI_{3-x}Cl_x$" Perovskite. Adv Funct Mater **24**, 7102–7108 (2014)
21. Xia, Y.D., He, W.Y., Chen, L., Meng, X.K., Liu, Z.G.: Field-induced resistive switching based on space-charge-limited current. Appl Phys Lett **90**, 1–4 (2007)
22. Lee, J.S., Lee, S., Noh, T.W.: Resistive switching phenomena: A review of statistical physics approaches. Appl Phys Rev **2**, 031303 (2015)
23. Azpiroz, J.M., Mosconi, E., Bisquertcd, J., Angelis, F.D.: Defect migration in methylammonium lead iodide and its role in perovskite solar cell operation. Energy Environ Sci **8**, 2118–2127 (2015)
24. Elumalai, N.K., Uddin, A.: Hysteresis in organic–inorganic hybrid perovskite solar cells. Sol Energ Mat Sol C **157**, 476–509 (2016)
25. Li, C., Guerrero, A., Zhong, Y., Huettner, S.: Origins and mechanisms of hysteresis in organometal halide perovskites. J Phys-Condens Mat **29**, 1–20 (2017)
26. Yamada, N., Ino, R., Ninomiya, Y.: Lead-free, air-stable hybrid organic–inorganic perovskite resistive switching memory with ultrafast switching and multilevel data storage. Chem Mater **28**, 4971–4981 (2016)
27. Zhu, X., Lee, J., Lu, W.D.: Iodine vacancy redistribution in organic–inorganic halide perovskite films and resistive switching effects. Adv Mater **1700527**, 1–8 (2017)
28. Liu, A., Zhu, H.H., Park, W.T., Kang, S.J., Xu, Y., Kim, M.G., Noh, Y.Y.: Room-Temperature Solution-Synthesized *p*-Type Copper(I) Iodide Semiconductors for Transparent Thin-Film Transistors and Complementary Electronics. Adv Mater **1802379**, 1–7 (2018)
29. Zi, M., Li, J., Zhang, Z.C., Wang, X.S., Han, J., Yang, X.P., Qiu, H.B. Z W andGong, Ji, Z.W., Cao, B.Q.: Effect of deposition temperature on transparent conductive properties of γ-CuI film prepared by vacuum thermal evaporation. Phys Status Solidi A **212**, 1466–1470 (2015)
30. Das, C., Wussler, M., Hellmann, T., Mayer, T., Jaegermann, W.: In situ xps study of the surface chemistry of mapi solar cells under operating conditions in vacuum. Phys Chem Chem Phys **20**, 17180–17187 (2018)
31. Liu, T., Su, P.Y., Liu, L., Wang, J., Feng, S., Zhang, J.J., Xu, R., Yang, H.B., Fu, W.Y.: An ionic compensation strategy for highperformance mesoporous perovskite solar cells: healing defects with tri-iodide ions in a solvent vapor annealing process. J Mater Chem A **7**, 353–362 (2019)
32. Guan, X.W., Hu, W.L., Haque, M.A., Wei, N.N., Liu, Z.X., Chen, A.T., Wu, T.: Light-responsive ion-redistribution-induced resistive switching in hybrid perovskite schottky junctions. Adv Funct Mater **28**, 1704665 (2018)
33. How, G.T.S., Talik, N.A., Kar, Y.B., Nakajima, H., Tunmee, S., Tong, G.B.: Multiple resistive switching behaviours of $CH_3NH_3PbI_3$ perovskite film with different metal electrodes. Appl Surf Sci **473**, 194–202 (2018)
34. Yoo, E.J., Lyu, M.Q., Yun, J.H., Kang, C.J., Choi, Y.J., Wang, L.Z.: Bifunctional resistive switching behavior in an organolead halide perovskite based Ag/$CH_3NH_3PbI_{3-x}Cl_x$/FTO structure. J Mater Chem C **4**, 7824 (2016)